Available online at www.sciencedirect.com
ScienceDirect
Journal of the European Ceramic Society 30 (2010) 1145–1150
www.elsevier.com/locate/jeurceramsoc

Electrophoretic deposition and characterization of Eu_2O_3 nanocrystal—Carbon nanotube heterostructures

S.V. Mahajan [a,b], J. Cho [c], M.S.P. Shaffer [d], A.R. Boccaccini [c], J.H. Dickerson [b,e,*]

[a] *Interdisciplinary Program in Materials Science, Vanderbilt University, Nashville, TN 37235, USA*
[b] *Vanderbilt Institute of Nanoscale Science and Engineering, Vanderbilt University, Nashville, TN 37235, USA*
[c] *Department of Materials, Imperial College, London SW7 2BP, UK*
[d] *Department of Chemistry, Imperial College, London SW7 2AZ, UK*
[e] *Department of Physics and Astronomy, Vanderbilt University, Nashville, TN 37235, USA*

Available online 22 September 2009

Abstract

Electrophoretic deposition (EPD) was employed to assemble a layered architecture of multi-walled carbon nanotube (CNT) mats and europium oxide nanocrystal (NC) films. CNT mats were produced via low field–high current EPD, while NC films were deposited via high field–low current EPD. The two EPD techniques were integrated in an alternating sequence to create CNT mat–NC film–CNT mat heterostructures with sharp interfaces. The EPD techniques produced uniformly porous CNT mats and densely packed NC films. Morphology and surface coverage of the films were investigated using scanning electron microscopy (SEM), while elemental characterization was performed using energy dispersive spectroscopy (EDS). Photoluminescence (PL) spectroscopy measurements were conducted on the NC suspension and the NC films to confirm film formation. Capacitance–voltage (CV) measurements were performed to probe energy-storage capabilities of the layered architecture.

Keywords: Films; Suspensions; Nanocomposites; Nanotubes; Eu_2O_3

1. Introduction

Research and development of composite architectures of carbon nanotubes (CNTs) and nanocrystals (NCs) is a continuously growing research field.[1–9] The interest is to integrate CNTs and NCs, taking advantage of their unique properties, into various architectures for next-generation magnetic, optical and energy-storage devices. An example architecture is a layered composite of CNTs and NCs with sharp interfaces, which is integral to existing and proposed devices such as supercapacitors and fuel cells. In electrochemical energy-storage devices, charges are stored on active electrodes that are isolated by a charge separator. Conducting materials are required for the active electrodes, and an electrical insulator is needed as a separating layer.[10] CNTs are known for their conductive properties and have been investigated as a material for electrodes in fuel cells and supercapacitors.[4,10] Europium oxide (Eu_2O_3) is known for its light emissive and electrically insulating properties.[11–13] Eu_2O_3 has been employed as a red emitter in field emission based display screens and has been proposed as a promising candidate material for high-k gate dielectrics for transistors.[11,12] The high dielectric constant ($k \sim 12$) of Eu_2O_3 makes it an ideal candidate for an electrically insulating separator layer in electrochemical energy-storage devices.[13] Also, the high dielectric constant of Eu_2O_3 facilitates using a thin film to achieve electrical insulation between active electrodes. These properties of CNTs and Eu_2O_3 motivate our investigation on integrating CNTs and Eu_2O_3 nanocrystals into a layered architecture for energy-storage device applications.

Implementation of Eu_2O_3 NC film as a separator between CNT layers is a possible architecture for device applications. The separator layer is typically thicker than 10 μm. Use of thinner separator layers would facilitate increased charge-storage per unit volume. The separator layer thickness can be reduced if a high-*k* dielectric material, such as Eu_2O_3, is used. It is important to achieve good electrical insulation when reducing the separator layer thickness. For the proposed prototype, production of a high quality layered structure of CNTs and NCs is required. The ability to deposit homogeneous layers of CNTs and NCs

* Corresponding author at: Department of Physics and Astronomy, Vanderbilt University, Nashville, TN 37235, USA. Tel.: +1 615 343 2957; fax: +1 615 343 7263.
E-mail address: james.h.dickerson@vanderbilt.edu (J.H. Dickerson).

0955-2219/$ – see front matter © 2009 Elsevier Ltd. All rights reserved.
doi:10.1016/j.jeurceramsoc.2009.08.016

on top of one another is vital to the successful development of functional layered architectures. Of the available film fabrication methods from nanoparticles, electrophoretic deposition (EPD) is one of the most promising techniques.[7,8] A degree of site selectivity, substantial thickness control, and homogeneous film microstructure at high deposition rates are among the attractive features of EPD.[14] CNTs and various semiconductor and oxide NCs have successfully been deposited to produce homogeneous films using EPD.[1,15–17] Further studies have employed EPD to fabricate layered architectures of CNTs and TiO_2/SiO_2 nanocrystals.[7,8] A CNT mat–Fe_3O_4 NC film–CNT mat heterostructure was fabricated recently using low field–high current and high field–low current EPD techniques.[9] Fe_3O_4 NCs were well dispersed in a non-polar medium (hexane), while CNTs were well dispersed in a polar medium (water). The significant difference in the electrical conductivities of the two media required two different EPD regimes. It was observed that the non-dispersibility of the CNTs in hexane prevented impregnation of the NCs inside the CNT mat during NC deposition, which facilitated the creation of sharp interfaces between the layers.

Here, we report for the first time the successful fabrication of the CNT mat–Eu_2O_3 NC film–CNT mat heterostructure for energy-storage device using the alternating low field–high current and high field–low current EPD technique. Homogeneous CNT mats were deposited from an aqueous CNT suspension, while Eu_2O_3 NC films were produced from NC suspension in hexane. Energy dispersive spectroscopy (EDS) and photoluminescence spectroscopy (PL) confirmed the deposition of the Eu_2O_3 NCs atop the CNT layer. Capacitance–voltage (CV) measurements verified the electrical insulating properties of the Eu_2O_3 NC film and potential energy-storage capabilities of the heterostructure.

2. Experimental

2.1. Materials synthesis

A chemical vapor deposition (CVD) technique was employed to grow multi-walled CNTs of approximately 50 nm diameter, as reported elsewhere.[18] Briefly, a ferrocene–toluene mixture was injected into a quartz tube furnace, which was filled with a hydrogen:argon (1:9) gas mixture and was maintained at 760 °C. Arrays of aligned CNTs formed on the inside surface of the quartz tube. Upon removal of the CNTs from the quartz tube's surface, the CNTs were purified with an acid-treatment.[17,18] The purification process involved refluxing 1 g of as-grown CNTs in a mixture of nitric acid (100% grade, 10 ml) and sulphuric acid (100% grade, 30 ml) at 120 °C for 30 min. Next, the CNTs were washed with de-ionized (DI) water until the suspension showed no changes in acidity. The aqueous CNT suspension was sonicated for a few hours and centrifuged at 3500 rpm for 15 min. The purified CNTs were employed for EPD.

Europium oxide (Eu_2O_3) nanocrystals of ~2.4 nm diameter were synthesized via a two-stage technique.[19] In the first stage, europium chloride hexahydrate ($EuCl_3{\cdot}6H_2O$) and sodium oleate ($CH_3(CH_2)_7CH{:}CH(CH_2)_7COONa$) were added to a water–ethanol–hexane mixture and heated at 70 °C for 4 h to produce the europium–oleate complex (Eu-oleate). The Eu-oleate, dispersed in hexane, was isolated using a separatory funnel. In the second stage, 0.50 mM Eu-oleate was mixed with 0.25 mM oleic acid in 7 ml tri-n-octylamine. The mixture was heated to ~350 °C and refluxed for 1 h to synthesize the Eu_2O_3 nanocrystals. The nanocrystals were isolated from the reaction mixture by a precipitation and centrifugation procedure. Ethanol was added to the reaction mixture to precipitate the nanocrystals, and the mixture was centrifuged at 3500 rpm for 30 min to isolate the nanocrystals. The nanocrystals were dispersed again in fresh hexane, after which the precipitation–centrifugation cycle was repeated. The nanocrystals were cleaned several times by this process before being employed for EPD.

2.2. Electrophoretic deposition (EPD)

316L grade stainless steel sheet, purchased from McMaster Carr, USA, were employed as the electrode materials for EPD. Electrodes, of size 25.0 mm × 12.0 mm × 0.2 mm, were cleaned with acetone and DI water. For EPD, a vertical parallel-plate configuration was employed. A typical EPD experiment comprised the application of dc voltage to the electrode pair and then insertion of the pair into the EPD suspension. Upon completion of the deposition, the electrode pair was extracted from the suspension. The electrodes were air-dried while maintaining an applied voltage to facilitate densification.[20] The deposits were classified into two regimes based on the applied electric field and current flowing through the EPD suspension, low field–high current and high field–low current.[9] The deposition current during EPD comprises two components, electrophoretic current and electrolytic current. The suspension medium controls the electrolytic component, while the suspended nanomaterials govern the electrophoretic component. The polar or non-polar nature of the suspension medium strongly controls the electrolytic current and hence, the overall deposition current. For a polar medium (e.g. water), large electrolytic current flows at low applied electric fields, which results in a large deposition current. In contrast, a negligible electrolytic current flows through a non-polar suspension (e.g. hexane) even at high electric fields, resulting in a small deposition current. Typically, a polar medium-based EPD falls under low field–high current regime, while a non-polar

Table 1
EPD parameters for CNTs and Eu_2O_3 nanocrystals (NCs).

Material	Suspension medium	Electrode spacing (mm)	Voltage (V)	Deposition time (min)	Drying time (min)
CNTs	Water	10	20	10	15
NCs	Hexane	2	1000	15	5

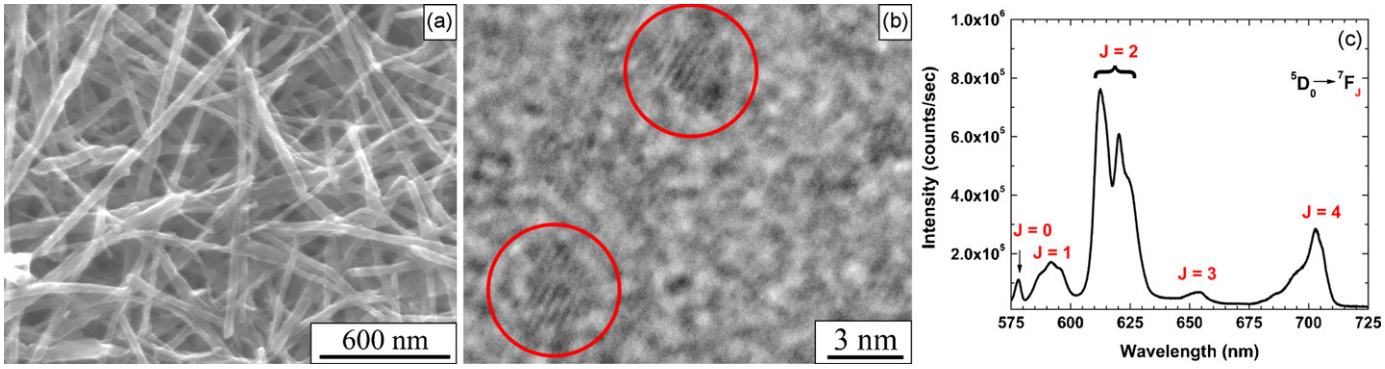

Fig. 1. (a) SEM image of CNTs, (b) TEM image and (c) photoluminescence spectrum of ~2.4 nm diameter Eu_2O_3 NCs.

medium-based EPD falls under high field–low current regime. In this study, well-dispersed suspensions of functionalized CNTs were prepared in water and suspensions of Eu_2O_3 NCs were prepared in hexane. Hence, the low field–high current and high field–low current regimes were employed for the EPD of the CNTs and Eu_2O_3 NCs, respectively. The parameters used for EPD are listed in Table 1.

An alternating sequence of EPD of CNTs and NCs was employed to produce CNT-NC layered heterostructures. First, a CNT mat was deposited on the steel electrode. Next, the CNT mat was used as an anode during the deposition of NCs. Subsequently, the NC-deposited CNT mat was employed as the anode for the deposition of the second CNT mat. Thus, CNT mat–NC film–CNT mat heterostructures were fabricated using this sequence.

2.3. Characterization

We analyzed the dimensions of the CNTs and the Eu_2O_3 nanocrystals using a Hitachi S-4200 field-emission scanning electron microscope (SEM) and a Philips CM 20 transmission electron microscope (TEM). Morphologies of the CNT and NC films were characterized using the SEM operating at the accelerating voltage of 10 kV. Elemental analyses of the EPD films were completed using energy dispersive spectroscopy (EDS). Photoluminescence (PL) measurements of the CNT mats and NC films were conducted using a Fluorolog-3 FL3-111 spectrophotofluorometer, equipped with a 450 W xenon lamp and a photomultiplier tube. Capacitance–voltage (CV) measurements were performed on a Signatone probe station using a Keithley 590 CV analyzer.

3. Results and discussion

Fig. 1 shows an SEM image of the EPD film of the purified CNTs atop a steel substrate, a TEM image of monodisperse 2.4 nm diameter Eu_2O_3 NCs, and a corresponding PL spectrum of the NCs. The average diameter of the purified CNTs was 50 nm, confirmed by SEM (Fig. 1(a)). The length of the purified CNTs varied between 1 and 2 μm. The acid-treatment process, performed to purify the CNTs, has the secondary effect of shortening the CNTs.[17,18] Fig. 1(b) shows a TEM image of the Eu_2O_3 nanocrystals of average core diameter ~2.4 nm. PL spectrum of the NCs, shown in Fig. 1(c), exhibits the characteristic emission peaks of Eu_2O_3 NCs. These emission peaks arise from the $^5D_0 \rightarrow {}^7F_{J=0-4}$ electron energy transitions within Eu^{3+} ions. We observed the dominant red emission (~611 nm and ~621 nm) signatures that are typical of the Eu_2O_3 nanocrystals.

A well-dispersed, aqueous suspension of purified CNTs was employed for EPD of CNT mats on metallic substrates following processing parameters optimized in previous experiments.[17] The negative charges on CNT surfaces were induced during the purification process as a consequence of the functionalization of the CNT surfaces with negatively charged, oxygen-containing acidic groups. Hence, purified CNTs deposited only on the anode (steel electrode) to produce a CNT mat. The morphology of the

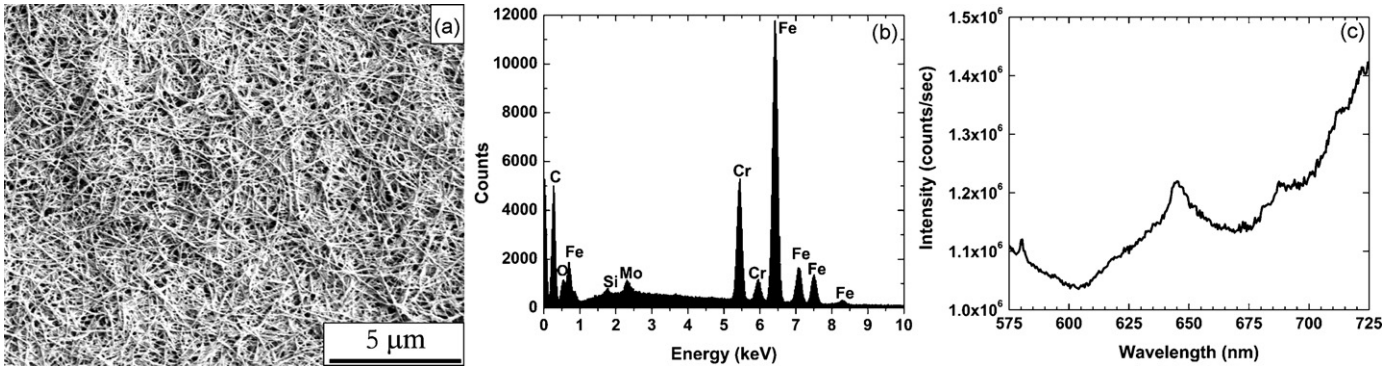

Fig. 2. (a) SEM image, (b) energy dispersive spectrum and (c) photoluminescence spectrum of the CNT mat.

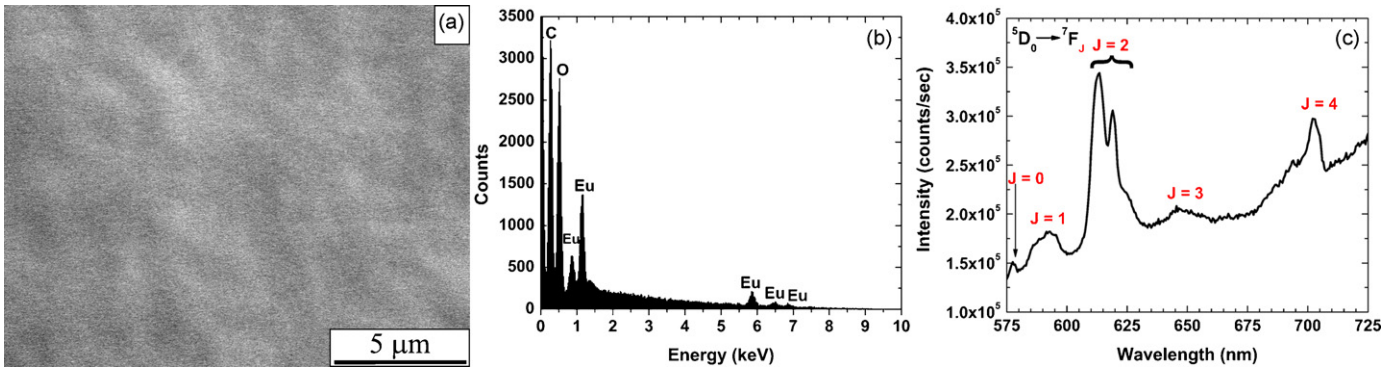

Fig. 3. (a) SEM image, (b) energy dispersive spectrum and (c) photoluminescence spectrum of the NC film deposited atop the CNT mat.

CNT mat was studied using SEM. Fig. 2(a) shows the SEM image of a CNT mat deposited on the steel electrode, using the parameters stated in Table 1. The majority of the CNTs lay flat in-plane with the electrode and are uniformly distributed within the mat. The CNTs within the mat are shown to be randomly oriented forming a porous network. Since the CNT mat was employed as an electrode to deposit the NCs, elemental and optical characterizations of the bare CNT mat were performed using energy dispersive spectroscopy and photoluminescence spectroscopy prior to the NC deposition. The energy dispersive spectrum of the CNT mat, deposited on the stainless steel substrate, is shown in Fig. 2(b). Besides the obvious detection of C, an oxygen peak was observed due to the presence of the oxygen-containing acidic groups on the surface of the purified CNTs. The iron, molybdenum, chromium, and silicon peaks were attributed to the underlying stainless steel electrode. The photoluminescence spectrum of the bare CNT mat, prior to the Eu_2O_3 NC deposition, was collected upon ultraviolet (UV) excitation and is shown in Fig. 2(c). Since the characteristic emission peaks of the Eu_2O_3 NCs lay in the 575–725 nm spectral region of the visible spectrum, the emission characteristics of the bare CNT mat were measured within the same spectral region. The CNTs exhibited a weak emission peak near 650 nm.

The Eu_2O_3 NCs, employed for the deposition, were capped with oleic acid and were well dispersed in the non-polar medium, hexane. Typically, charges on the nanocrystals, suspended in a non-polar solvent, are induced due to the adsorption of uncharged ligands, desorption of ionized ligands, and/or ion exchange between the ligand and NC surface.[21–26] Ensembles of surface charge states can produce electrically neutral, positive, and negative NCs.[27] Positively and negatively charged nanocrystals can be deposited on the cathode and anode, respectively. The Eu_2O_3 nanocrystals were deposited on top of the CNT mat via the high field–low current EPD method. The CNT mat-coated stainless steel electrode was employed as the anode during EPD.

Scanning electron microscopy, energy dispersive spectroscopy, and photoluminescence spectroscopy techniques confirmed the deposition of the Eu_2O_3 NCs atop the CNT mat. Fig. 3(a) shows the SEM image of the anode. A smooth and continuous NC film is visible, which covers the CNT mat entirely. All the pores present on the surface of the CNT mat were filled by the NCs, forming a continuous film. Previous studies using iron oxide NCs implemented multiple subsequent depositions of NCs to enhance the surface coverage of the NCs on top of the CNT mat.[9] In the present case, complete surface coverage was achieved during a single deposition of Eu_2O_3 NCs, which was likely due to a small size of the NCs. Smaller nanocrystals tend to have higher surface charge due to larger surface-to-volume ratio, engendering higher electrophoretic mobility.[28] After deposition, the morphology and contour of the underlying porous CNT mat was no longer visible. The energy dispersive spectrum, as seen in Fig. 3(b), confirmed the presence of europium, oxygen, and carbon on the anode, as expected for the oleic acid, CNTs, and Eu_2O_3 NCs present. The PL spectrum of the anode, shown in Fig. 3(c), has the characteristic emission peaks of Eu_2O_3 nanocrystals. The similarity of the spectrum of the film to that of sub-3 nm Eu_2O_3 NCs in suspension (Fig. 1(c)) suggests that EPD does not change the luminescence spectrum of the NCs.

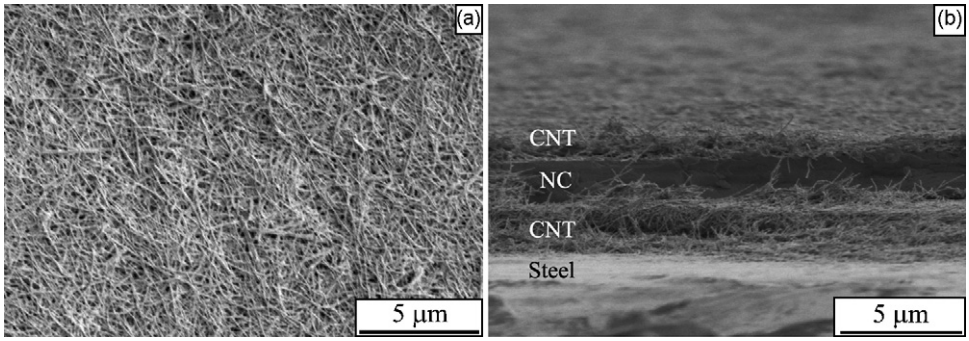

Fig. 4. (a) Top view SEM image and (b) side view SEM image of a CNT mat–NC film–CNT mat heterostructure.

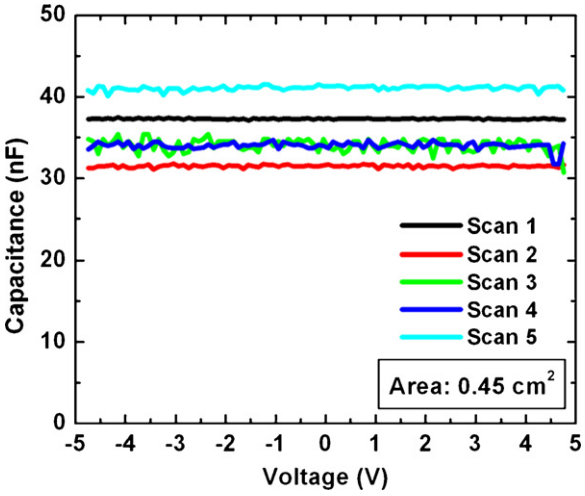

Fig. 5. Capacitance–voltage (CV) characteristics of a CNT mat–NC film–CNT mat heterostructures.

Thus, SEM images, EDS, and PL measurements confirmed the deposition of the homogeneous Eu_2O_3 NC film atop the CNT mat.

In parallel experiments, the NC-coated CNT mat was employed as the anode to deposit a second CNT mat in order to produce the CNT mat–NC film–CNT mat architecture. Fig. 4 shows the top view and side view SEM images of the heterostructure. The electrode with the heterostructure was cut in its center to obtain a clear cross-sectional view of said heterostructure. The morphology of the second CNT mat (Fig. 4(a)) was similar to that of the first CNT mat (Fig. 2(a)). However, a significant difference in the thickness of the two mats was observed for the same EPD configuration and deposition parameters. The first CNT mat was ~2 μm thick, while the second mat was ~500 nm thick, as shown in Fig. 4(b). During the second CNT deposition, a part of the applied voltage dropped across the preexisting, low-conductivity CNT mat–NC film architecture. Hence, the effective EPD electric field was reduced, leading to the thinner CNT mat. This result suggests that the thickness of the second CNT mat can be tuned by varying EPD parameters. Fig. 4(b) shows the separating, Eu_2O_3 NC film between the two CNT mats, which was ~2 μm thick. The sharp interface between the NC film and the CNT mat is visible. The NCs deposited only on the top surface of the CNT mat and did not penetrate inside the mat, forming a sharp interface. This outcome is in contrast to results on EPD of CNT/TiO_2 nanoparticle composites, where TiO_2 nanoparticles were seen to penetrate the upper layer of the porous CNT mat.[8] The non-dispersibility of CNTs in hexane prevented impregnation of the NC dispersion inside the mat, which facilitated a sharp interface formation. Thus, high quality CNT mat–NC film–CNT mat heterostructures with sharp interfaces were reproducibly formed using the low field–high current and high field–low current EPD method.

Electrical characteristics of the CNT mat–NC film–CNT mat heterostructures were probed using CV measurements. Fig. 5 shows five representative CV curves of the heterostructure, which exhibit a relatively stable, consistent capacitance over the entire ±5 V voltage range. An average capacitance of 35.4 ± 3.7 nF was measured for the system. Such a CV response is typical of a metal–insulator–metal (MIM) capacitor.[29] This CNT mat–NC film–CNT mat architecture mimics the MIM structure and, thus, exhibits a comparable CV response. Our CV measurements confirmed that the two CNT mats were electrically insulated from one another and that charges were stored in this arrangement. These results confirm that a CNT mat–NC film–CNT mat architecture could be employed as a structure for an energy-storage device.

4. Conclusions

Multi-layered architectures, comprising carbon nanotubes and europium oxide nanocrystals, were successfully fabricated on steel substrates via electrophoretic deposition. Low field–high current EPD facilitated the deposition of uniform porous CNT mats. Densely packed Eu_2O_3 nanocrystal films were deposited via high field–low current EPD. The two EPD techniques were employed in an alternating sequence to build the layered architecture. The nanocrystals deposited homogenously on the CNT mat producing a continuous film. The non-dispersibility of the CNTs in hexane prevented impregnation of the NC suspension into the CNT mat, leading to a sharp interface between the layers. Energy dispersive spectroscopy and photoluminescence spectroscopy confirmed the deposition of the Eu_2O_3 nanocrystals onto the CNT mat. Characteristic luminescence peaks of the Eu_2O_3 NC film were identical to those of the NC suspension. A second CNT mat, deposited atop the NC film, was thinner than the first CNT mat deposited directly on the steel substrate. The increased voltage drop between the electrodes due to the CNT mat–NC film architecture led to this effect. CV measurements of the CNT mat–NC film–CNT mat structure confirmed electrical insulation between the two CNT mats and the charge-storage capabilities of the structure. The successful development of energy-storage device prototypes, comprised of layered CNT mat–Eu_2O_3 NC film heterostructure, demands further research efforts in this area.

References

1. Boccaccini, A. R., Cho, J., Roether, J. A., Thomas, B. J. C., Minay, E. J. and Shaffer, M. S. P., Electrophoretic deposition of carbon nanotubes. *Carbon*, 2006, **44**, 3149–3160.
2. Cava, C. E., Possagno, R., Schnitzler, M. C., Roman, P. C., Oliveira, M. M., Lepiensky, C. M. *et al.*, Iron- and iron oxide-filled multi-walled carbon nanotubes: electrical properties and memory devices. *Chem. Phys. Lett.*, 2007, **444**, 304–308.
3. Georgakilas, V., Gournis, D., Tzitzios, V., Pasquato, L., Guldi, D. M. and Prato, M., Decorating carbon nanotubes with metal or semiconductor nanoparticles. *J. Mater. Chem.*, 2007, **17**, 2679–2694.
4. Girishkumar, G., Hall, T. D., Vinodgopal, K. and Kamat, P. V., Single wall carbon nanotube supports for portable direct methanol fuel cells. *J. Phys. Chem. B*, 2006, **110**, 107–114.
5. Kalbac, M., Frank, O., Kavan, L., Zukalova, M., Prochazka, J., Klementova, M. *et al.*, Heterostructures from single-wall carbon nanotubes and TiO_2 nanocrystals. *J. Electrochem. Soc.*, 2007, **154**, K19–K24.
6. Li, W. Z., Liang, C. H., Zhou, W. J., Qiu, J. S., Zhou, Z. H., Sun, G. Q. *et al.*, Preparation and characterization of multiwalled carbon nanotube-supported platinum for cathode catalysts of direct methanol fuel cells. *J. Phys. Chem. B*, 2003, **107**, 6292–6299.

7. Chicatun, F., Cho, J., Schaab, S., Brusatin, G., Colombo, P., Roether, J. A. *et al.*, Carbon nanotube deposits and CNT/SiO_2 composite coatings by electrophoretic deposition. *Adv. Appl. Ceram.*, 2007, **106**, 186–195.
8. Cho, J., Schaab, S., Roether, J. A. and Boccaccini, A. R., Nanostructured carbon nanotube/TiO_2 composite coatings using electrophoretic deposition (EPD). *J. Nanopart. Res.*, 2008, **10**, 99–105.
9. Mahajan, S. V., Hasan, S. A., Cho, J., Shaffer, M. S. P., Boccaccini, A. R. and Dickerson, J. H., Carbon nanotube-nanocrystal heterostructures fabricated by electrophoretic deposition. *Nanotechnology*, 2008, 19.
10. Du, C. S. and Pan, N., High power density supercapacitor electrodes of carbon nanotube films by electrophoretic deposition. *Nanotechnology*, 2006, **17**, 5314–5318.
11. Shionoya, S. and Yen, W. M., *Phosphor Handbook*. CRC Press, Boca Raton, 1999.
12. Dakhel, A. A., Characteristics of deposited Eu_2O_3 film as a thick gate dielectric for silicon. *Eur. Phys. J. Appl. Phys.*, 2004, **28**, 59–64.
13. Singh, M. P., Shalini, K., Shivashankar, S. A., Deepak, G. C., Bhat, N. and Shripathi, T., Microstructure, crystallinity, and properties of low-pressure MOCVD-grown europium oxide films. *Mater. Chem. Phys.*, 2008, **110**, 337–343.
14. Besra, L. and Liu, M., A review on fundamentals and applications of electrophoretic deposition (EPD). *Prog. Mater. Sci.*, 2007, **52**, 1–61.
15. Islam, M. A., Xia, Y. Q., Steigerwald, M. L., Yin, M., Liu, Z., O'brien, S. *et al.*, Addition, suppression, and inhibition in the electrophoretic deposition of nanocrystal mixture films for CdSe nanocrystals with gamma-Fe_2O_3 and Au nanocrystals. *Nano Lett.*, 2003, **3**, 1603–1606.
16. Islam, M. A., Xia, Y. Q., Telesca, D. A., Steigerwald, M. L. and Herman, I. P., Controlled electrophoretic deposition of smooth and robust films of CdSe nanocrystals. *Chem. Mater.*, 2004, **16**, 49–54.
17. Corni, I., Ryan, M. P. and Boccaccini, A. R., Electrophoretic deposition: From traditional ceramics to nanotechnology. *J. Eur. Ceram. Soc.*, 2008, **28**, 1353–1367.
18. Singh, C., Shaffer, M. S. and Windle, A. H., Production of controlled architectures of aligned carbon nanotubes by an injection chemical vapour deposition method. *Carbon*, 2003, **41**, 359–368.
19. Mahajan, S. V. and Dickerson, J. H., Synthesis of monodisperse sub-3 nm RE_2O_3 and Gd_2O_3: RE^{3+} nanocrystals. *Nanotechnology*, 2007, 18.
20. Hasan, S. A., Kavich, D. W., Mahajan, S. V. and Dickerson, J. H., Electrophoretic deposition of CdSe nanocrystal films onto dielectric polymer thin films. *Thin Solid Films*, 2009, **517**, 2665–2669.
21. Fowkes, F. M. and Pugh, R. J., Steric and electrostatic contributions to the colloidal properties of nonaqueous dispersions. In *ACS Symp Series 240*. Am. Chem. Soc., Washington, DC, 1984, pp. 331–354.
22. Morrison, I. D., Electrical charges in nonaqueous media. *Colloids Surf. A: Physicochem. Eng. Aspects*, 1993, **71**, 1–37.
23. Morrison, I. D. and Ross, S., *Colloidal Dispersions: Suspension, Emulsions, and Foams*. Wiley-Interscience, New York, 2002.
24. Fowkes, F. M., General discussion. *Discuss. Faraday Soc.*, 1966, **46**, 246–247.
25. Pugh, R. J., Matsunaga, T., Fowkes, F. M. and The Dispersibility, Stability of carbon-black in media of low dielectric-constant. 1. Electrostatic and steric contributions to colloidal stability. *Colloids Surf.*, 1983, **7**, 183–207.
26. Tamaribuchi, K. and Smith, M. L., Charge-determining species in nonaqueous solvents. *J. Colloid Interface Sci.*, 1966, **22**, 404-&.
27. Shevchenko, E. V., Talapin, D. V., Kotov, N. A., O'brien, S. and Murray, C. B., Structural diversity in binary nanoparticle superlattices. *Nature*, 2006, **439**, 55–59.
28. Yuan, H., Cheow, P.-S., Ong, J. and Toh, C.-S., Characterization of the electrophoretic mobility of gold nanoparticles with different sizes using the nanoporous alumina membrane system. *Sens. Actuators B*, 2008, **134**, 127–132.
29. Mikhelashvili, V., Eisenstein, G. and Lahav, A., High capacitance density metal-insulator-metal structure based on Al[sub 2]O[sub 3]—HfTiO nanolaminate stacks. *Appl. Phys. Lett.*, 2007, **90**, 013506–13513.